*Research Article*

# Regions of Different Confinement in Low-Dimensional Al$_y$In$_x$Ga$_{1-x-y}$N Quantum Structures

**A. Gröning, V. Pérez-Solórzano, M. Jetter, and H. Schweizer**

*4. Physikalisches Institut, Universität Stuttgart, Pfaffenwaldring 57, 70569 Stuttgart, Germany*

The optical properties of metal-organic vapor phase epitaxy grown Al$_y$In$_x$Ga$_{1-x-y}$N quantum dot structures have been studied by time-resolved photoluminescence experiments. We investigated the recombination dynamics of the photo-exited carriers in dependence of the growth parameters such as aluminium flow and the duration of the growth interruption after the dot deposition. Our results confirm the presence of localized states, where the degree of localization is strongly dependent on the growth conditions. To describe this behavior, we propose a band structure with coupled potentials for these nanostructures. Finally, we demonstrate state filling to prove the zero-dimensional character of the strongly localized states in our quaternary quantum dots.

## 1. INTRODUCTION

Quaternary nitride alloys have been studied intensively in the last years because of the significantly enhanced quantum efficiency in comparison to AlGaN with the similar Al-content [1, 2], being an advantage for applications in the ultraviolet spectral range [3]. The possibility of separately adjustment of the lattice constant and the band gap that offer the quaternary material [4, 5] allows the growth of layers lattice matched to GaN and a reduction of the piezoelectric fields at the GaN/AlInGaN interfaces.

The enhanced optical properties of AlInGaN layers at room temperature have been attributed to the existence of In-rich nanoclusters, which are responsible for the confinement of the electron-hole pairs [6]. Moreover an unstable mixing region has been predicted for the quaternary nitride compounds [7], and *ab initio* calculations showed that the presence of Al in InGaN catalyses the phase separation process leading an In-rich phase [8].

In our experiments, we use this enhanced phase separation to overcome the existing difficulties in the formation of nitride quantum dots (QD) via the Stranski-Krastanow (SK) growth mode [9]. The growth of self-assembled QDs becomes more favourable if we modify the strain and the surface energy of the underlying barrier layer [10]. Our previous work [11, 12] described the 3D-island formation by introducing Al during the growth of InGaN and determined the influence of the growth parameters on the structural prop-erties of the quantum dots. In this paper, we present results on the carrier dynamics in these quaternary QDs. We will show that localized structures with different confinement energies are present, depending on the growth parameters. The zero-dimensional character of these nanostructures has been proven by the observation of state filling.

## 2. EXPERIMENTAL PROCEDURES

The Al$_y$In$_x$Ga$_{1-x-y}$N nanostructures were deposited on a 1 $\mu$m high-quality GaN buffer layer grown on sapphire (0001) by low-pressure (100 mbar) metal-organic vapor-phase epitaxy (MOVPE). After cleaning the substrate in a hydrogen atmosphere and the deposition of the AlN nucleation layer, the GaN buffer was grown at 1120°C. The reactor temperature was subsequently reduced to 760°C, and the main dilution was changed from hydrogen (H$_2$) to nitrogen (N$_2$), ensuring a completely H$_2$-free atmosphere. Typical molar fluxes were 19 $\mu$mol/min of Triethylgallium (TEGa), and 20 $\mu$mol/min of Trimethylindium (TMIn), whereas the Trimethyaluminium (TMAl) flow was varied between 1.5 $\mu$mol/min and 5.7 $\mu$mol/min. The ammonia (NH$_3$) flow was increased to 9000 sccm in order to ensure enough N-supply at this low growth temperature [13]. The growth deposition was interrupted for up to 60 seconds after the deposition of the dot layer to examine the changes in the surface morphology. To avoid the chemical dissociation of the layer, the process takes place under NH$_3$ flow.
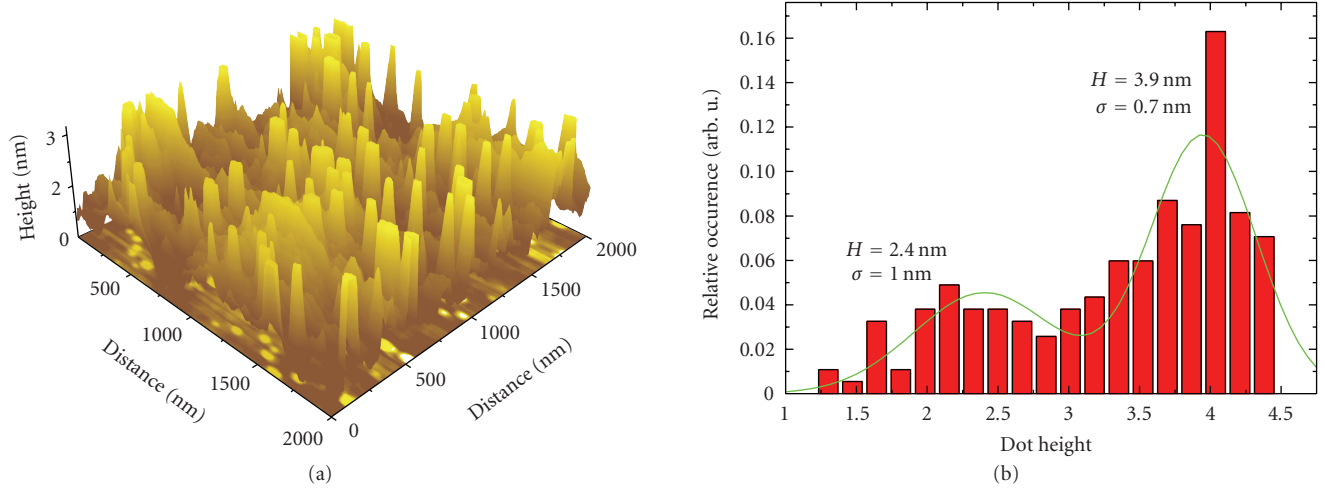
(a)

(b)

FIGURE 1: (color online). (a) AFM scan of a quaternary sample. The dot density is approximately $4.6 \cdot 10^9$ dots/cm². (b) Distribution of the dot heights. A well-defined bimodal distribution with heights of 2.4 nm and 3.9 nm, respectively, is visible.

For the optical experiments the samples were capped with 25 nm GaN grown at the same temperature as the dot layer. Details about the growth of AlInGaN-QDs have been published elsewhere [11, 12]. For comparison we grew three ternary InGaN samples with an In flow between 16 $\mu$mol/min and 40 $\mu$mol/min, respectively.

The topology of the surfaces was examined using a topometrix explorer atomic force microscopy (AFM) in contact mode. Figure 1(a) shows an AFM image of a quaternary sample with a TMAl flux of 3.5 $\mu$mol/min. A distinct morphology of three-dimensional islands is visible in this figure. The maximum height of these dots is around 4.5 nm and the density is $4.6 \cdot 10^9$ dots/cm². A detailed analysis of the surface leads to the statistical height distribution of the nanostructures displayed in Figure 1(b). We observe a bimodal distribution of the dot height. The major part of these islands exhibits a height around 3.9 nm, but there are still quantum dots present with a height around 2.4 nm. This bimodal distribution is often seen in self-assembled quantum dots and could also be observed in other material systems.

To determine the optical properties, photoluminescence (PL) measurements were performed using a frequency-doubled Ti:Sapphire laser at a wavelength around 355 nm with 200 fs pulse width. The luminescence was dispersed in a 0.32 m Jobin-Yvon monochromator and detected by a fast multichannel plate photomultiplier tube by time-correlated single-photon counting. Additionally, time-resolved measurements were performed using a streak camera with 10 picosecond time resolution. The samples were placed on a cold finger cryostat.

## 3. RESULTS

A time-integrated PL spectrum of an AlInGaN sample grown at 800°C is displayed in Figure 2(a). A clear emission peak at 3.32 eV with a small shoulder at 3.22 eV was measured. In order to investigate the carrier dynamics, we analyzed the de-

cay of the luminescence. Figure 2(b) shows a typical luminescence transient where one can clearly see the nonexponential decay of the intensity. This behavior is quite common and well known especially in the nitride material system [14]. We can fit the decay behavior by a stretched exponential model known from heavily disordered materials [15]:

$$\frac{I(t)}{I_0} = \exp\left[ -\left(\frac{t}{\tau^*}\right)^{\beta} \right], \quad (1)$$

where $\tau^*$ is the characteristic life of the decay and $\beta$ the stretching parameter that gives a measure of the degree of disorder in the material. This stretched exponential behavior can be interpreted by energetic or topological disorder [15]. Carriers confined in different spatial regions can diffuse due to excitation from localized to excited states (energetic disorder) or by hopping among localized states (topological disorder). The characteristic life $\tau^*$ can be evaluated from the time where $I(t)/I_0 = \exp(-1)$ and $\beta$ from a linear fit to $\ln(-\ln(I(t)/I_0))$ versus $\ln(t)$ as shown in the inset of Figure 2(b). We see here that a linear relation does not fit perfectly, indicating that $\beta$ is not a constant. For most luminescence decays the slope in the plot $\ln(-\ln(I(t)/I_0))$ versus $\ln(t)$ deviates from a constant especially at short times [14, 16–18]. We interpret this observation as follows: after the excitation, the photo-generated excitons thermalize and occupy extended states from where they rapidly relax towards lower lying localized states, resulting in the fast initial decay of the PL transient. The excitons which reached the localized states now redistribute much slower which can be described by the stretched exponential. At least this stretched exponential model gives us the access to the characteristic lifetime of the PL decay. Figure 2(a) shows the spectral dependence of the luminescence time constant $\tau^*$. The decrease of $\tau^*$ with increasing energies is caused by the rise of transfer processes from QDs with smaller localization energy or from quantum well states. The decrease of the decay time with increasing
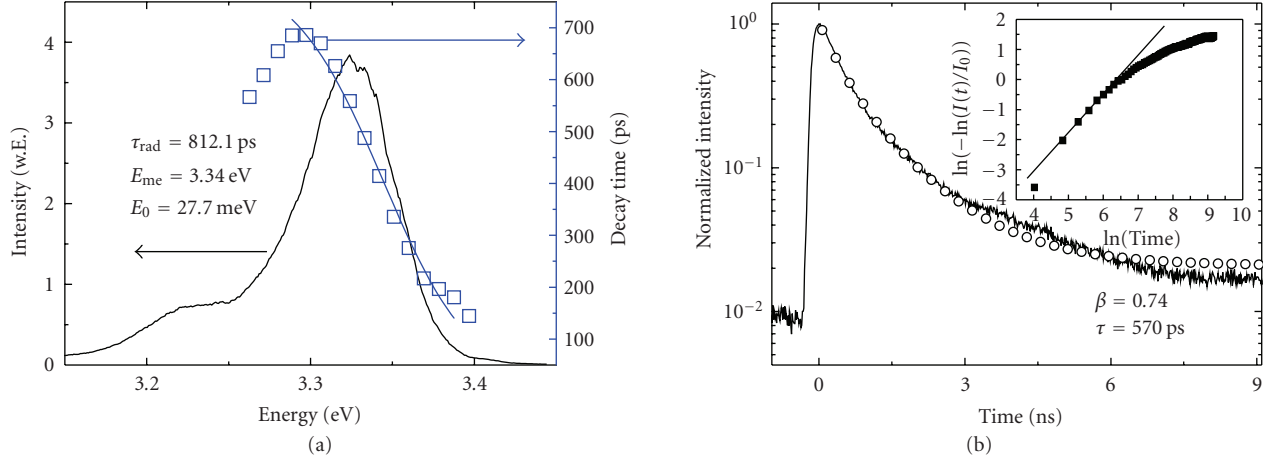
FIGURE 2: (a) Time-integrated PL spectrum (black) and the decay time (blue) as a function of the monitored emission energy. The blue line is a theoretical fit after the model of Gourdan and Lavallard [19]. $E_{me}$ is the mobility edge, $E_0$ the localization energy, and $\tau_{rad}$ the radiative life time. (b) Normalized intensity of the photoluminescence versus time. The inset shows $\ln(-\ln(I(t)/I_0))$ versus log time from where $\beta$ can be derived.

energy therefore indicates the rising contribution of nonradiative recombination of the localized states. The radiative lifetime of these localized excitons as well as their mobility properties and average binding energy can be determined using the model proposed by of Gourdon and Lavallard [19]. The PL decay time for localized excitons as a function of the spectral position, assuming the density of localized states is proportional to $\exp(-E/E_0)$, can be described by

$$\tau(E) = \frac{\tau_{rad}}{1 + \exp\left[(E - E_{me})/E_0\right]}, \qquad (2)$$

where $\tau_{rad}$ is the radiative lifetime, $E_{me}$ is the energy for which the radiative decay equals the lateral transfer time, and $E_0$ is the characteristic energy for the density of states. $E_{me}$ signifies the change from the three-dimensional localized QD states to quantum well states with higher exciton mobility (often interpreted as the mobility edge). Above this energy the propagation of the excitons is more probable than their radiative decay. $E_0$ is a measure of the average localization energy of the QDs. Using (2) we obtained a radiative decay time of $\tau_{rad} \sim 810$ ps, an $E_{me} \sim 3.34$ eV, and an average binding energy of $E_0 \sim 28$ meV. We observed that the PL is emitted at energies below $E_{me}$ which is a clear indication for the QD origin of the luminescence. At lower energies of the emission band we find a deviation from the model. This is attributed to an increasing confinement of the excitons in the QDs with higher localization energy and therefore with a higher electron-hole wave function overlap, resulting in a decrease of the decay times with lower energy as can be seen in Figure 2(a).

To further analyze the character of the PL emission of our different samples, we define the energy difference between $E_{me}$ and the PL peak energy $E_{PL}$ as a measure of the dimensionality of the structures. Negative differences of $(E_{me} - E_{PL})$ imply emission from quantum well states, while positive differences $(E_{me} - E_{PL})$ can be attributed to three-

dimensional localized states. Figure 3(a) displays $(E_{me} - E_{PL})$ for the three InGaN reference samples versus the TMIn flow. From the growth conditions of these structures we expect just emission from weakly localized states, respectively, quantum wells. As can be seen in Figure 3(a) all energy differences $(E_{me} - E_{PL})$ have negative values, confirming the expectations from the growth. With increasing indium content the magnitude trends even higher, indicating an enhanced two-dimensional character. In comparison, $(E_{me} - E_{PL})$ for three different quaternary AlInGaN structures are plotted in Figure 3(b) versus the TMAl flow. Here we clearly see that with increasing Al content $(E_{me} - E_{PL})$ changes from negative to positive values, indicating a transition from two-dimensional character of the emission to quantum dot luminescence. This picture is also supported by the fact that atoms like Al or Si act as antisurfactants during the start of the growth, resulting in an enhanced formation of three-dimensional islands. Our further investigations concentrate now on these quaternary QD structures.

The PL spectrum of the QD ensemble without growth interruption (Figure 4) consists of a broad luminescence around 2.9 eV. The complete emission band from 2.6 eV to 3.2 eV can be fairly well described by a superposition of three peaks at 2.86 eV, 2.93 eV, and 3.07 eV, respectively. In the spectral dependence of the PL decay times in Figure 4 we can clearly distinguish two pronounced $\tau(E)$ resonances, corresponding to the peaks at 2.86 eV and 2.93 eV. For the peak at 3.07 eV the exact behavior of the $\tau(E)$ curve is unclear, so we focus on the two resonances with lower energy. From (2) we extract the radiative lifetime $\tau_r$, the mobility edge $E_{me}$, and the characteristic energy $E_0$ for these two peaks. The obtained values are $\tau_1 = 560$ picoseconds, $E_{me} = 2.91$ eV, $E_0 = 36$ meV for the luminescence peak at $E_{PL} = 2.86$ eV, and $\tau_2 = 480$ picoseconds, $E_{me} = 2.98$ eV, $E_0 = 38$ meV for the emission at $E_{PL} = 2.93$ eV. We determine the nature of the luminescence again by determining the energy
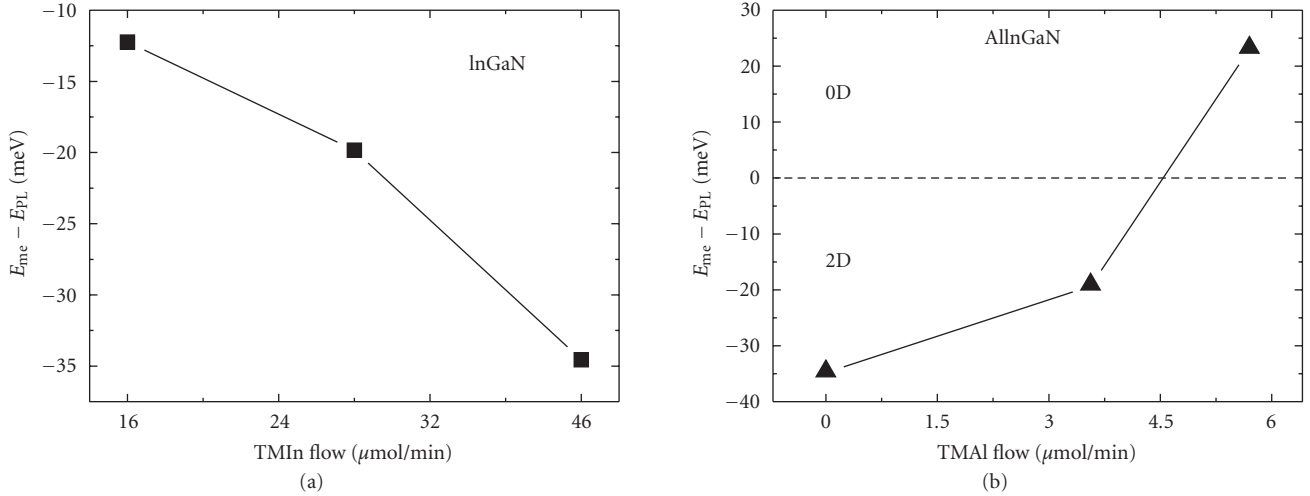
FIGURE 3: (a) Difference between $E_{me}$ (mobility edge) and PL energy $E_{PL}$ as a measure of dimensionality of the structure. $E_{me} - E_{PL}$ plotted versus the TMIn flow for different ternary samples grown at 800°C. (b) $E_{me} - E_{PL}$ plotted versus the TMAl flow for different quaternary samples grown at 800°C. The dashed line indicates a transition from two-dimensional character of the emission to quantum dot luminescence.
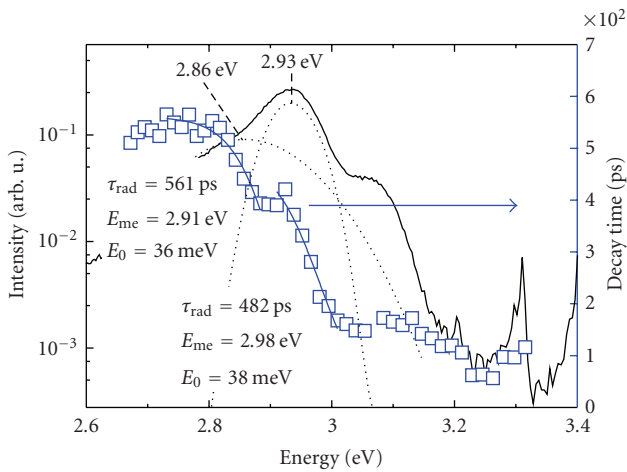


FIGURE 4: Time-integrated PL spectrum (black) and the PL decay time (blue squares) versus the emission energy. $E_{me}$ is the mobility edge, $E_0$ the localization energy, and $\tau_{rad}$ the radiative life time. The spectrum consists of two different emission peaks at 2.69 eV and 2.82 eV. We use the theoretical fit by (2).
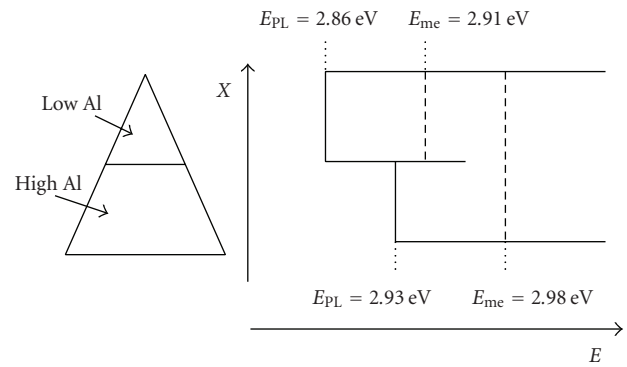


FIGURE 5: (a) pyramidal shape of a nitride dot with higher aluminum incorporation at the base than in the apex. In the vertical axis is the growth direction of the dot. (b) step shape of the band structure to explain the emission properties. In the horizontal direction is the energy axis of the band structure, vertical axis is also the growth direction.

differences ($E_{me} - E_{PL}$). The calculated values are 48 meV and 45 meV, respectively. The positive sign is again an indication for the emission from localized states or rather QDs. To explain these two different emission peaks from localized states inside the QD ensemble luminescence band, we suggest a model in which the QD consists of regions with different indium and aluminum content. It is well known that quaternary AlGaInN structures tend to phase separation and to build a long-range ordered superlattice of high and low Al-containing layers [5]. A quantum dot posses regions of different strain due to its characteristic geometric. A pyramidal QD for example exhibits a strain difference between the apex and the base of the pyramid [20], which favours the incorpo-

ration of one atom species more than the others. This would lead to nanoislands with different composition profile. This was also previously observed for example in Ga$_x$In$_{1-x}$ P/GaP QDs, where the dots exhibit an In-rich apex surrounded by a Ga-rich base [21]. In our case, we have higher aluminium incorporation at the base than in the apex, assuming a pyramidal structure as for ternary nitride dots [22]. From these considerations, we determined the step-shaped band structures shown in Figure 5 to explain the emission properties of our samples. The low energy peak at 2.86 eV is the emission from a region with less aluminium and correspondingly more indium, while the luminescence at 2.93 eV is from an Al-rich part of the QD. Between the two propose levels, we suggest
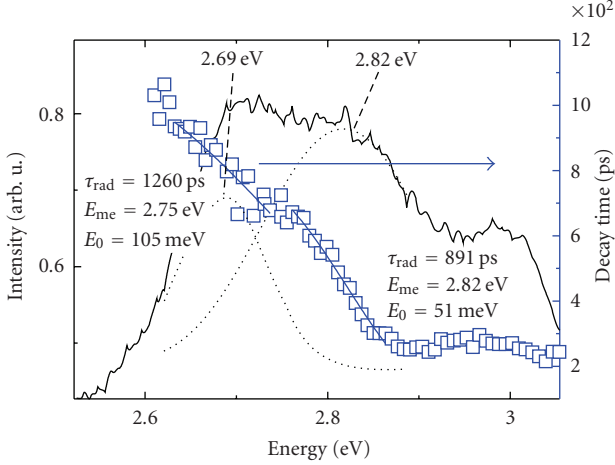
FIGURE 6: Time-integrated PL spectrum (black) and the PL decay time (blue squares) versus the emission energy for a quaternary sample with growth interruption. $E_{me}$ is the mobility edge, $E_0$ the localization energy, and $\tau_{rad}$ the radiative life time. It consists of two different emission peaks at 2.86 eV and 2.93 eV. We use the theoretical fit by (2).



FIGURE 7: Time evolution of the spectrum for the sample with growth interruption (red: high intensity, blue: low intensity).

an energetic barrier as in Figure 5 to be the reason for band gap discontinuities. From (2) we have obtained the values of $E_{me}$ where the lateral transfer time equals the recombination of the excitons. This means that the carriers mainly relax via $E_{me}$ into the radiative states $E_{PL}$. As $E_{PL}$ of the Al-rich part of the dot has nearly the same value as $E_{me}$ of the In-rich section, we expect that the carriers relax via the Al-rich phase to the lower energy part of the QD. The differences in the radiative decay times of $\tau_1$ = 560 picoseconds for the emission at 2.86 eV and $\tau_2$ = 480 picoseconds for the peak at 2.93 eV also support the existence of an additional relaxation channel for the aluminum rich phase. For the luminescence at 3.07 eV in Figure 4, we can extend our model and attribute this emission to the region close to the buffer layer, where Al acts as antisurfactant and is therefore heavily incorporated inside the nanostructure.

The situation is now changed if we focus on the emission properties of a quantum dot sample with growth interruption. From this growth interruption we expect a ripening of the QD and an indium enhancement. As Figure 6 demonstrates, the main part of the emission is shifted to lower energies which indicates the redistribution of In during the growth interruption. Again the emission band can be fitted by three peaks, now at 2.68 eV, 2.81 eV, and 3.0 eV, respectively. From the spectral dependence of the decay times we also find two $\tau(E)$ resonances for the two low energy luminescence peaks. The obtained values of $\tau_r$, $E_{me}$, and $E_0$ according to (2) are shown as inset in Figure 6. The energy differences ($E_{me} - E_{PL}$) of 70 meV, respectively, 10 meV confirm once more emission from localized states. We observed that now the difference of values of ($E_{me} - E_{PL}$) is much larger than for the sample in Figure 4. If we take again our model of the QD with different composition into account, we see that the carriers are much stronger confined in the In-rich region at 2.68 eV than in the Al-rich region at 2.81 eV. This is
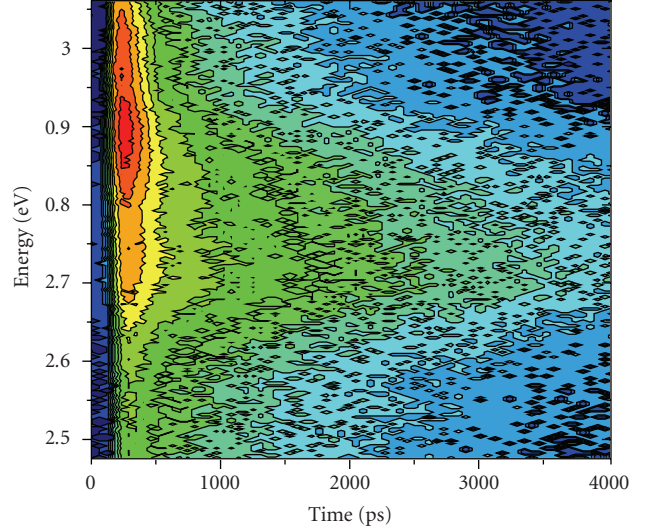
also supported by the high localization energy $E_0$ = 105 meV of the low-energy peak compared to $E_0$ = 51 meV for the second one. Also in this case of quantum dots with regions of strong and weak confinement our assumption of a coupled system inside the QD seems to be valid. One would expect that the radiative lifetime in the strong confined region is short because of the better electron-hole wave function overlap. In our example, then high In-content in the strongly confined region and the piezoelectric effect in the nitrides causing an electric field increase the lifetime up to 1.26 nanoseconds.

The time evolution of the luminescence of this sample is shown in Figure 7. Directly after the excitation pulse, the carrier density is high in the QD ensemble and decreases with the radiative decay times of the involved states. As one can clearly see the luminescence band shows at short times a redistribution of the PL dominating states rather than a blue shift of the whole spectrum as it would be expected for screening of the electric field. With decreasing carrier density the lowest energy state becomes more pronounced. This effect is called state filling and it is an indication for the presence of quantum dots in this AlInGaN structure.

## 4. CONCLUSION

We have used time-integrated and time-resolved PL measurements to determine the emission characteristics of our AlInGaN nanostructures. Based on these analyses, we developed a model of coupled systems to describe the time-resolved luminescence properties. Using a model of phase separation during the growth and the formation of an indium rich, respectively, aluminum rich part inside the QD, the measured luminescence band could be well described. The existence of QDs in our structures was independently confirmed by state filling.

## REFERENCES

[1] J. P. Liu, B. S. Zhang, M. Wu, et al., "Structural and optical properties of quaternary AlInGaN epilayers grown by MOCVD with various TMGa flows," *Journal of Crystal Growth*, vol. 260, no. 3-4, pp. 388–393, 2004.

[2] Y. Liu, T. Egawa, H. Ishikawa, et al., "High-temperature-grown quaternary AlInGaN epilayers and multiple quantum wells for ultraviolet emission," *Journal of Crystal Growth*, vol. 264, no. 1–3, pp. 159–164, 2004.

[3] H. Hirayama, "Quaternary InAlGaN-based high-efficiency ultraviolet light-emitting diodes," *Journal of Applied Physics*, vol. 97, no. 9, Article ID 091101, 19 pages, 2005.

[4] Y. Liu, T. Egawa, H. Ishikawa, and T. Jimbo, "Growth and characterization of high-quality quaternary AlInGaN epilayers on sapphire," *Journal of Crystal Growth*, vol. 259, no. 3, pp. 245–251, 2003.

[5] Y. Kobayashi, Y. Yamauchi, and N. Kobayashi, "Structural and optical properties of AlGaInN/GaN grown by MOVPE," *Japanese Journal of Applied Physics, Part 1*, vol. 42, no. 4B, pp. 2300–2304, 2003.

[6] C. H. Chen, Y. F. Chen, Z. H. Lan, et al., "Mechanism of enhanced luminescence in $In_xAl_yGa_{1-x-y}N$ quaternary epilayers," *Applied Physics Letters*, vol. 84, no. 9, pp. 1480–1482, 2004.

[7] T. Matsuoka, "Calculation of unstable mixing region in wurtzite $In_{1-x-y}Ga_xAl_yN$," *Applied Physics Letters*, vol. 71, no. 1, pp. 105–106, 1997.

[8] M. Marques, L. K. Teles, L. M. R. Scolfaro, L. G. Ferreira, and J. R. Leite, "Microscopic description of the phase separation process in $Al_xGa_yIn_{1-x-y}N$ quaternary alloys," *Physical Review B*, vol. 70, no. 7, Article ID 073202, 4 pages, 2004.

[9] R. A. Oliver, M. J. Kappers, C. J. Humphreys, and G. A. D. Briggs, "Growth modes in heteroepitaxy of InGaN on GaN," *Journal of Applied Physics*, vol. 97, no. 1, Article ID 013707, 8 pages, 2005.

[10] K. Nakajima, T. Ujihara, S. Miyashita, and G. Sazaki, "Effects of misfit dislocations and AlN buffer layer on the GaInN/GaN phase diagram of the growth mode," *Journal of Applied Physics*, vol. 89, no. 1, pp. 146–153, 2001.

[11] V. Pérez-Solórzano, A. Gröning, H. Schweizer, and M. Jetter, "Growth of self-assembled $Al_xIn_yGa_{1-x-y}N$ quantum dots by MOVPE," *Journal of Crystal Growth*, vol. 272, no. 1–4, pp. 186–191, 2004.

[12] V. Pérez-Solórzano, A. Gröning, H. Schweizer, and M. Jetter, submitted to *Physica Status Solidi*.

[13] M. Kamp, M. Mayer, A. Pelzmann, and K. J. Ebeling, "Fundamentals, material properties and device performances in GaN MBE using on-surface cracking of ammonia," *MRS Internet Journal of Nitride Semiconductor Research*, vol. 2, 1997, article 26.

[14] T. Bartel, M. Dworzak, M. Strassburg, A. Hoffmann, A. Strittmatter, and D. Bimberg, "Recombination dynamics of localized excitons in InGaN quantum dots," *Applied Physics Letters*, vol. 85, no. 11, pp. 1946–1948, 2004.

[15] H. Scher, M. F. Shlesinger, and J. T. Bender, *Physics Today*, vol. 41, p. 26, 1991.

[16] M. Pophristic, F. H. Long, C. Tran, I. T. Ferguson, and R. F. Karlicek Jr., "Time-resolved photoluminescence measurements of InGaN light-emitting diodes," *Applied Physics Letters*, vol. 73, no. 24, pp. 3550–3552, 1998.

[17] Y. J. Sun, O. Brandt, S. Cronenberg, et al., "Non-polar $In_xGa_{1-x}N/GaN(11\bar{0}0)$ multiple quantum wells grown on $\gamma$-LiAlO$_2$(100) by plasma-assisted molecular-beam epitaxy," *Physical Review B*, vol. 67, no. 4, Article ID 041306, 4 pages, 2003.

[18] B. M. Weon, J.-L. Lee, and J. H. Je, "A unified decay formula for luminescence decays," *Journal of Applied Physics*, vol. 98, no. 9, Article ID 096101, 3 pages, 2005.

[19] C. Gourdon and P. Lavallard, "Exciton transfer between localized states in $CdS_{1-x}Se_x$ alloys," *Physica Status Solidi (B)*, vol. 153, no. 2, pp. 641–652, 1989.

[20] D. Bimberg, M. Grundmann, and N. N. Ledentsov, *Quantum Dot Heterostructures*, John Wiley & Sons, Chichester, NH, USA, 1999.

[21] G. J. Beirne, M. Jetter, M. Rossi, et al., "Optical studies of GaInP/GaP quantum dots," *Journal of Luminescence*, vol. 102-103, pp. 1–6, 2003.

[22] V. Pérez-Solórzano, Y. Kobayashi, M. Jetter, et al., "Initial experiments to obtain self-assembled GaInN quantum islands by MOVPE," *Physica Status Solidi (A)*, vol. 192, no. 2, pp. 412–416, 2002.